Comparison of $^{13}C_2H_4$ and $^{13}CH_4$ Injection through Graphite and Tungsten Limiters in TEXTOR

S. Brezinsek[1], A. Kreter[1], R. Ding[1], T. Hirai[2], A. Kirschner[1], V. Philipps[1]
A. Pospieszczyk[1], U. Samm[1], B. Schweer[1], O. Schmitz[1], K. Sugiyama[3]
T. Tanabe[4], Y. Ueda[5] and the TEXTOR team

[1] *Institut für Energieforschung - Plasmaphysik, Forschungszentrum Jülich, Association EURATOM-FZJ, Trilateral Euregio Cluster, Germany*

[2] *ITER Organisation, Cadarache Centre, F-13108 St. Paul-lez-Durance, France*

[3] *Max-Planck-Institut für Plasmaphysik, EURATOM Association, 85748 Garching bei München, Germany*

[4] *Interdisciplinary Graduate School of Engineering Science, Kyushu University, Japan*

[5] *Graduate School of Engineering, Osaka University, Osaka 565-0871, Japan*

Abstract

Experiments in the plasma-wall interaction facility at TEXTOR have been carried out to compare (i) the local transport of $^{13}CH_4$ and $^{13}C_2H_4$ injected through a gas aperture implemented in spherical limiters made of polycrystalline tungsten and fine-grain graphite, and (ii) the properties of local deposited carbon layers on the polished limiter surface. Each limiter was positioned in the scrape-off layer and exposed to ten identical ohmic deuterium discharges of $4s$ length - accumulating 40 plasma seconds. The injection rates were normalised to the amount of injected ^{13}C. The analysis is twofold: spectroscopy was applied to follow up in-situ the observable hydrocarbon break-up products (C_2, CD, C^+, and C^{2+}), and post-mortem analysis was used to determine the ^{13}C deposition efficiency. The penetration depths of hydrocarbon break-up products in the plasma were determined. Significant CH emission was observed in front of W limiter prior to injection. The ^{13}C deposition efficiency shows a dependence on both the limiter material and on the injected hydrocarbon species.

PACS: 52.70.Kz, 52.40.Hf, 52.25.Vy, 52.55.Fa, 33.20.Lg

1 Introduction

The choice of the divertor plasma-facing material is one of the outstanding issues for ITER, which will first operate in pure hydrogen before entering with deuterium and tritium the activated operation phase. The initial divertor will be made of plasma-facing components made of carbon-fibre composite *(CFC)* and tungsten to allow large flexibility and highest power handling during transients in the start phase of ITER, thereby *CFC* is proposed for the high heat and particle flux region at the target plates and tungsten at the baffle region and the dome area [1]. Carbon can be eroded at the target plate, transported and deposited as carbon layer away from the strike-zone on either *CFC* or tungsten plasma-facing component. These carbon layers, which can vary in their properties such as e.g. the $H : C$ ratio, are built-up depending on the local plasma parameters [2,3], the surface conditions (e.g. surface material and roughness) [4] and the divertor geometry and magnetic configuration [5]. In the case of ITER the amount of mobilisable tritium, which is limited to $700g$, co-deposited with carbon and beryllium is critical from the point of view of safety and can inhibit further operation when cleaning/removal actions are not performed [6]. Though, W is foreseen as plasma-facing material in the divertor for the activated phase, a short campaign with *CFC* and W, leading to an early demonstration of significant fusion power, is not excluded. Recent experiments have gained a better understanding of material migration [7-9], but the role of higher hydrocarbons in the migration process and their impact on carbon layer properties and in particular on the fuel content is uncertain due to lack of experiments which can distinguish between layers induced by methane and higher hydrocarbons.

Experiments in the plasma-wall interaction (PWI) test facility at TEXTOR have been carried out to compare both the local transport and catabolism of $^{13}C_2H_4$ and $^{13}CH_4$ injected through a gas inlet implemented in the spherical limiter, and to compare the properties

of the deposited carbon layers on the polished limiter surface. Additionally, the set of two tungsten and two graphite limiters used in this comparative experiment allowed to study the impact of the limiter substrate on the deposition efficiency. In four subsequent experiments each limiter was positioned in the PWI test facility at the location of the near scrape-off layer and exposed to the TEXTOR edge plasma for about 40 plasma seconds. In each experiment a comparable amount of ^{13}C atoms - present in the two different hydrocarbon gases - has been locally injected and a fraction of it deposited on the limiter surface. The molecular break-up and the carbon transport in the plasma has been studied in-situ with the aid of hydrocarbon spectroscopy and the local deposition pattern on the limiters has been characterised post mortem by visual observation and nuclear reaction analysis (NRA). This contribution summarises the complementary experimental observations, spectroscopy and surface analysis, and provides a set of reference data to benchmark the erosion and deposition Monte-Carlo code ERO with respect to the impact of higher hydrocarbons on the local transport and deposition efficiency. Previous benchmark experiments have aimed only on methane injection, transport, and deposition [2], on the impact of the substrate material and the surface roughness on the deposition efficiency [4,10], and, most recently, on the verification of the molecular data base for the break-up of higher hydrocarbons in the plasma [11,12]. This set of 4 experiments focuses on the direct experimental comparison of destruction of methane and ethene injected into plasma and the resulting local deposition efficiency of carbon layers on the graphite or tungsten substrate.

The paper is structured in the following way: section 2 gives information about the four experiments including information about the limiter preparation, the experimental set-up, the edge plasma conditions, as well as, the applied in-situ diagnostics. Section 3 describes the spectroscopic observation of hydrocarbon break-up products CH, C_2, C^+, C^{2+} in the light of the molecular CH Gerö and C_2 Swan band as well as of different transitions of CII

and $CIII$ providing e.g. the 2D distributions in front of the limiter, the radial penetration profiles into the plasma, and the time evolution. Section 4 deals with the post mortem analysis, in particular with the ^{13}C deposition efficiency pattern on the limiter surfaces. The summary including conclusive remarks is given in section 5.

2 Experimental set-up and plasma conditions

Two spherical graphite limiters, made of fine-grain graphite (EK98), and two spherical tungsten limiters, made of polycrystalline tungsten, were installed subsequentially in the PWI facility in TEXTOR [13]. The graphite limiters, shown in figure 1 and described in detail with respect to geometrical properties e.g. in [14], have been polished to a surface roughness of $R_a = 0.1\mu m$, comparable to the one of the unpolished tungsten, which minimises the impact of surface roughness on the deposition efficiency [3]. Each limiter was positioned in the scrape-off layer (SOL) with the tip one centimetre behind the last-closed flux surface (LCFS) in the erosion-dominated zone and exposed to ten identical deuterium discharges (plasma current: $0.35MA$, toroidal magnetic field: $2.25T$, line-averaged central density $2.5 \times 10^{19} m^{-3}$, ohmic heating power $0.3MW$) without additional heating. Thereby, the LCFS is determined by the main toroidal belt limiter to $r = 46cm$ - the minor radius of TEXTOR. The ohmic discharges were highly reproducible and no wall conditioning was applied between discharges. The cumulated plasma exposure at the current and density flattop between $0.8s$ and $\sim 4.5s$ amounts to about $40s$ per installed limiter. Each limiter was electrically pre-heated to a temperature of $T \simeq 670K$; the limiter temperature remains constant during the plasma exposure as measurements by thermocouples –positioned $2mm$ below the limiter surface– confirmed.

Local gas injection has been performed through a circular injection aperture of $2mm$ diameter located $15mm$ away from the limiter tip in toroidal direction and centred in poloidal direction. This corresponds also to the location of the largest ion flux impact in the spherical limiter geometry, therefore, it will be referred to as the strike-zone. The injection was applied between $1.5s$ and $3.0s$, however, the gas effuses continuously after closing the pneumatic valve in $2m$ distance and exceeds the duration of the current flattop phase. Reference gas injection pulses into the TEXTOR vacuum vessel for each gas and limiter combination were performed to determine the fraction of gas injected within the plasma flattop phase. ^{13}C labelled methane ($^{13}CH_4$) and ethene ($^{13}C_2H_4$) were applied for the injection in order to be able to distinguish the deposition of injected carbon from the background carbon ^{12}C atoms. Moreover, the injection of $^{13}C_2H_4$ and $^{13}CH_4$ was performed into deuterium plasmas; the hydrogen from the break-up of the injected hydrocarbon can therefore be spectroscopically distinguished from the deuterium background plasma. The injection rate for $^{13}C_2H_4$ has been lowered by a factor of two to normalise the amount of injected ^{13}C atoms with respect to the $^{13}CH_4$ injection. The maximum injection rate reaches $1.0 \times 10^{19} s^{-1}$ methane molecules per second. Though no significant difference in the edge parameters for the two injected species was observed, a moderate local disturbance due to the injection cannot be excluded. Comparable injection rates in previous experiments indicated a disturbance of less than 15% in the local electron temperature and electron density [11].

The edge plasma parameters electron density n_e and temperature T_e were determined at the outer midplane with the aid of a He-beam diagnostic using the line ratio of three neutral He lines [15]. Typical plasma edge profiles at $t = 2.0s$ are depicted in figure 2 for two representative discharges with either $^{13}CH_4$ or $^{13}C_2H_4$ injection through graphite limiter. The variation in edge profiles are within the error bars of the diagnostic method indicating the good reproducibility of the edge plasma conditions. The deuterium recycling flux has

been determined spectroscopically by observation of D_α at the strike-zone [13]. Assuming a recycling coefficient of one; the impinging deuterium ion flux density is typically about $D^+ = 6.5 \times 10^{22}\ ions\ s^{-1}m^{-2}$.

3 Spectroscopic analysis of hydrocarbon break-up products in the edge plasma

The light emission of spectroscopically observable break-up products of hydrocarbon molecules delivers information about the dissociation and ionisation processes during the catabolism in the plasma; in particular the 2D distribution, the penetration depth profiles, and the fraction of the different break-up products as function of time. These topics have been studied simultaneously with a set of complementary spectroscopic systems in the visible range: 2D cameras with narrowband interference filters [13], spectrometer systems with integral or radial resolved information [11] and a high resolution spectrometer [16]. However, with the given set of spectroscopic systems it is impossible to distinguish between optical transitions from species containing ^{13}C and ^{12}C, thus, the two injected species containing ^{13}C are spectroscopically equivalent to regular methane and ethene.

3.1 CH and CD A-X band emission in discharges with $^{13}C_2H_4$ injection

The 2D distribution of the Gerö or A-X band photon flux density in front of a graphite limiter (upper images) and a tungsten limiter (lower images) is depicted in figure 3a. The data was recorded with an image intensified CCD camera (Proxitronic 4L) equipped with a

narrowband interference filter ($[430.7nm+/-1.0]nm$) which covers a significant wavelength span of both the CD A-X band head at $430.9nm$ and the CH A-X band head at $431.4nm$ in discharges with ethene injection. A large fraction of the Q and R branches of the first two main diagonal transitions which are degraded to the blue wavelength region are included in the wavelength span; total fluxes related to the full electronic transition can be determined by taking into account the ro-vibrational population (here: $\simeq 3500K$) leading to a correction factor of about 2.8 [11].

The first image in each row represents the reference, the intrinsic CD emission at the strike-zone in the pure deuterium plasma before the injection - averaged between $1.0s$ and $1.4s$. The second image shows the sum of intrinsic CD emission and extrinsic CH emission resulting from the molecular break-up of the injected $^{13}C_2H_4$ - averaged between $2.8s$ and $4.4s$. The difference is shown in the third image and reflects mainly the extrinsic CH emission due to the local injection at the strike-zone. This extrinsic CH emission is –as shown in the image– almost independent of the limiter material and reflects the bare catabolism of the injected $^{13}C_2H_4$ in the plasma.

Integration of the CD/CH $A-X$ band photon flux density in a narrow stripe of $5mm$ in toroidal direction at the gas injection location provides the penetration depth of CD/CH in front of the tungsten and graphite limiter at the strike-zone (figure 3b). The extrinsic penetration depth profiles are similar. The intrinsic and total profiles indicate differences in the absolute intensity between graphite and tungsten which will be discussed below.

Figure 3c provides the time evolution of the CD/CH A-X band photon flux density integrated over the full observation chord in the corresponding discharges with $^{13}C_2H_4$ injection through graphite and tungsten limiter, respectively. The flattop phase with constant plasma parameters including the reference phase before injection, the opening time of the valve and the post effusive time are indicated. The pure extrinsic contribution to the photon flux is

marked by the area above the dashed lines. It is remarkable, that the CD photon flux in the reference phase in front of the graphite and tungsten limiters differs only by 30% with the higher flux, as expected, in the graphite case [17]. A possible explanation for the CD emission in front of the tungsten limiter is the appearance of a transient carbon layer induced by the impinging carbon flux of about 3% to 4% from the plasma background. Erosion of this transient carbon layer due to chemical sputtering causes the CD emission. In the case of graphite, both chemical sputtering of the bare substrate and from a transient carbon layer, comparable to the one on the tungsten, leads to the local emission of CD at the erosion zone. Additionally, the time evolution of the spatially integrated photon fluxes of the C_2 d-a band, the CII doublet at $426.7nm$ and the $CIII$ transition at $465.0nm$ are depicted in figure 3c. These carbon photon fluxes behave qualitative similar to the CH/CD photon flux in both the reference and injection phase. Directly volume integrated emission has also been recorded in addition to spectroscopically filtered data with a set of fibre-coupled compact spectrometer observing the spectral range between $350nm$ and $950nm$, providing a comparable time evolution of molecular transitions, CII and $CIII$ transitions as well as of the CI multiplet at $909.5nm$. The spectral integrity of the applied interference filters has been verified with the aid of a fibre-coupled high resolution spectrometer observing the spectral range between $375nm$ and $675nm$ without gap at once and integrating the light emission over the flattop phase.

3.2 2D emission pattern of break-up products: $^{13}C_2H_4$ vs. $^{13}C_2H_4$ injection

Figure 4 shows the emission distribution of transitions of extrinsic hydrocarbon break-up products (CH, C_2, C^+ and C^{2+}) during the catabolism of injected $^{13}C_2H_4$ (upper images)

and $^{13}CH_4$ (lower images) in deuterium plasma. This spatial distribution is resolved in radial and toroidal direction and integrated in poloidal direction over the limiter. The photon flux densities were recorded, as previously mentioned, with an intensified CCD camera equipped with narrowband interference filter for the C_2 Swan band ($[516.5 \pm 0.75]nm$), the CII transition at $[426.7 \pm 0.5]nm$ and the $CIII$ transition at $[465.0 \pm 1.5]nm$.

The extrinsic $CH\ A-X$ photon flux, obtained by spatial integration of the first image in each row, differs by a factor 2.4 between the discharge with methane and ethene injection under consideration of the slightly different injection pulse shape, ethene effuses slower than methane along the $2m$ connection pipe in the PWI facility, and thus, the exact normalisation to the amount of introduced ^{13}C atoms. This difference in the $CH\ A-X$ photon flux is comparable with previous experiments with hydrocarbon injection through gas inlets under similar plasma conditions [11] where the ratio of effective inverse photon efficiencies normalised to the amount of carbon atoms in the hydrocarbon molecule was determined to 2.6. This discrepancy is caused by the different production rate of the CH radical from the break-up of methane and ethene. However, the almost identical $CIII$ photon flux confirms that the overall production of carbon is, as expected, comparable for both injected species though some ions escape from the observation volume.

The distribution of the $C_2\ d-a$ emission during ethene and methane injection differs strongly. The localised emission close to the surface in the ethene case is due to the break-up process of the injected species, providing as final molecular species C_2. The distribution in the methane case, where a direct C_2 production is negligible [18], is likely a result of a secondary effect: re-erosion of a transient carbon layer induced by the hydrocarbon injection.

3.3 Penetration depth profiles of hydrocarbon break-up products

The penetration depth is a characteristic measure of the break-up due to dissociation and ionisation of hydrocarbon species entering a high temperature, ionising plasma and is used to benchmark the atomic and molecular data base implemented in the erosion and deposition codes used at present [11,17]. An imaging spectrometer system in Czerny Turner arrangement (Acton SpectraPro 500, focal length: $0.5m$, grating: $1200l/mm$, resolving power $R = 6000$ [11]) with the entrance slit imaged onto the gas inlet embedded in the spherical limiter was applied to determine the penetration depth profiles. The observation volume in front of the limiter is of rectangular shape, with the light emission integrated about $1mm$ in toroidal direction at the gas injection location, extended about $90mm$ in radial direction, spatially resolved by the spectrometer system (radial dispersion of $0.0137mm/pixel$), and integrated along the complete poloidal extension of the limiter. Two spectral regions including in (i) the CH/CD Gerö band head at $431.4nm$ and the CII doublet at $426.7nm$, and in (ii) the C_2 Swan band head at $516.5nm$ and the CII multiplet at $515.0nm$ were radially resolved recorded during the extrinsic phase with $^{13}CH_4$ and $^{13}C_2H_4$ injection, respectively, in front of the graphite and tungsten limiter, respectively. Fig. 5a shows for each combination of limiter material and injection species the spectral region (i) in the top row and region (ii) in the bottom row. Spectra were measured during the gas injection phase with subtraction of reference spectra recorded in the reference phase prior to the injection; these difference spectra represent therefore the bare light emission caused by extrinsic species. Note that, all spectra were recorded without neutral density filter with exception of the two spectra showing spectral region (i) during $^{13}CH_4$ injection where filter with transmission $T = 0.3$ were deployed to avoid saturation of the Gerö band and the CII doublet. The stronger Gerö band emission confirms the higher CH production rate in the case of $^{13}CH_4$ with respect to

$^{13}C_2H_4$ injection, as mentioned in the previous section. The maximum intensity of the CII emission at $426.7nm$ depends on the type of injected hydrocarbon species whereas almost no difference can be observed for the CII multiplet at $515.0nm$ for all 4 cases. A possible explanation for the difference in the CII transitions is the dissociation into different molecular ions or into excited states depending on the origin hydrocarbon molecule; a similar behaviour has been observed in [11] and [19].

The corresponding normalised penetration depth profiles of the four observed optical transitions, $CH\ A-X$ band, the $C_2\ d-a$ band heads, and the two CII transitions, are depicted in figure 5b. The CH penetration depth profile is in all four cases comparable and the corresponding penetration depth defined as one e-folding length of the intensity starting at the emission maximum lies between $0.44 \pm 0.01cm$. The C_2 penetration depth profile differs for the two injected species independent of the limiter material indicating the different origin of the C_2 dimer. The penetration depth determined by the break-up of the injected $^{13}C_2H_4$ molecule amounts to $0.38 \pm 0.01cm$. The minor C_2 emission in the case of $^{13}CH_4$ injection is caused by re-erosion of a transient in-situ built carbon layer during the injection leading to a release of higher hydrocarbons. The corresponding penetration depth amounts $0.49 \pm 0.01cm$. This difference is reflected in the emission pattern of C_2 shown in figure 4.

The penetration depth profile of the CII multiplet at $515.0nm$ shows a slight difference between the graphite and tungsten limiter case. The penetration depth amounts $1.32cm$ in the tungsten case and $1.10cm$ in the graphite case. In contrast, for the CII doublet at $426.7nm$, no clear dependence on the surface material can be seen, but the difference between methane and ethene injection is obvious. A shift of the emission maximum towards the plasma and a profile broadening with increase of the ionisation stage is observable for both injected species.

In the case of the tungsten limiters also different WI transitions, as the multiplet at $429.5nm$

interfering the Gerö band and at $505nm$ interfering the tail of the Swan band, were observed and identified as marked in figure 5a. The appearance of WI in this difference spectra shows clearly that additional physical sputtering of W takes place during the hydrocarbon injection which increases the W impurity flux by about a factor 2 with respect to the reference phase. This sputtering is most probably caused by bombardment of the tungsten limiter by energetic break-up fragments of the injected species. Detailed analysis of the tungsten sputtering is subject of a forthcoming paper and out of the scope of this contribution.

4 Post mortem analysis of locally deposited carbon layers

Post mortem analysis of the limiter surface is a complementary method to spectroscopy to describe the hydrocarbon tracer experiment. The figure of merit is the ^{13}C deposition efficiency on the limiter surface, i.e. the amount of deposited ^{13}C related to the number of injected ^{13}C atoms induced by either $^{13}C_2H_4$ or $^{13}CH_4$ injection. The deposition pattern on the limiter after plasma exposures is depicted in figure 1. Hard amorphous carbon layers are formed on the surfaces with a typical deuterium content of about $10\% - 20\%$. The local ^{13}C deposition close to the injection hole is in all cases separated by a net erosion zone from the ^{12}C deposition by the background plasma. The separation extends much larger for tungsten than for graphite and indicates the impact of the limiter material on the local flux balance; the balance between the carbon outflux, folded with the deposition efficiency of carbon on graphite or on tungsten, and the carbon erosion flux caused by the incident ion flux either on graphite or on a deposited carbon layer (on tungsten).

The optical inspection of the ^{13}C deposits on the four spherical limiters provides first infor-

mation about differences between, on the one hand tungsten and graphite substrates, and on the other hand $^{13}C_2H_4$ and $^{13}CH_4$ injections. The visible ^{13}C deposition area on the tungsten limiters is about half of the size of the one on the graphite limiters. Differences in the deposition area are less pronounced for the injected hydrocarbon species; the deposition zone is about 1/3 smaller in the case of $^{13}C_2H_4$ with respect to $^{13}CH_4$ injection. The transition between deposition and erosion-dominated regions is sharp in the case of tungsten limiters and slightly smoothed in the case of graphite limiters. With this respect, no difference can be observed between the two injected gases. The elongated shape of the ^{13}C layer, observed in all four cases (figure 6a), is caused by both the spherical limiter geometry and the direction of the local carbon transport. The latter is defined by the direction of the SOL plasma flow combined with the $E \times B$ drift. The difference in the angle between the direction of the magnetic field and the axis of widest extension of the deposited layer, indicated by lines in figure 6a, can be observed for the two injected species: the angle is about 10° larger for the $^{13}C_2H_4$ injections, thus, a smaller impact of the SOL flow on the deposition direction can be assumed for the heavier hydrocarbon.

Nuclear reaction analysis was applied to all limiter surface deposits to determine the integral amounts of deposited carbon isotopes and co-deposited deuterium, their depth and surface distributions on the surface. The absolute areal densities of ^{13}C, ^{12}C and D were measured with a $2.5MeV$ ^3He-beam; the protons from the $^{13}C(^3He,p)^{15}N$ and $D(^3He,p)^4He$ reactions were detected with a large angle particle counter equipped with a stopper foil for filtering out backscattered ^3He ions. NRA was performed for the entire deposition area close to the injection aperture with a lateral resolution of about $2mm$ in toroidal and poloidal direction. Figure 6a shows the ^{13}C areal density for all limiter and hydrocarbon injection combinations. In all cases is the maximum areal density close to the injection location. The ^{13}C areal density distribution is more peaked around the injection aperture for the $^{13}C_2H_4$ injection than

for the $^{13}CH_4$ injection. The distribution extends wider and is spread on the surface in the case of $^{13}CH_4$. This observation is confirmed in figure 6b, which shows the ^{13}C areal density along the axis of widest extension of the deposited films. The distribution of deuterium from the plasma background follows ^{13}C. The distribution of hydrogen from the injection cannot be determined by NRA.

The integral of the ^{13}C areal density over the complete layer extension normalised to the amount of injected ^{13}C atoms provides the deposition efficiency. The experiment reproduces the previously found material dependence of the deposition efficiency for comparable surface roughness [20] showing a deposition efficiency for tungsten of 0.8% and for graphite of 1.7%, which corresponds to a deposition efficiency ratio of 0.47 for $^{13}CH_4$. It also confirms the behaviour for the $^{13}C_2H_4$ injection with a deposition efficiency of 1.2% for tungsten and 2.1% for graphite; the corresponding ratio amounts 0.57. However, the ^{13}C deposition efficiency depends also on the type of injected hydrocarbon species: the ratio of the deposition efficiency for $^{13}CH_4$ and $^{13}C_2H_4$ amounts 0.80 for graphite and 0.67 for tungsten. The hydrocarbon species with higher mass leads to a significant stronger local ^{13}C deposition likely caused by different break-up products which have both a higher sticking probability and a lower mobility with respect to break-up products in the methane reference case.

5 Summary and conclusion

Comparative experiments in the PWI test facility at TEXTOR were performed to determine (i) the local transport of $^{13}CH_4$ and $^{13}C_2H_4$ injected through an aperture implemented in spherical limiter, and (ii) the properties of locally deposited carbon layers on the surface of the fine-grain graphite and polycrystalline tungsten limiter, respectively. The hydrocarbon

break-up in the plasma was analysed in-situ by spectroscopy and the deposited layer on the surface was studied ex-situ by post mortem analysis.

Main results and conclusions from spectroscopy are:

- The 2D distribution of break-up products is documented for both injected species by imaging spectroscopy. The integral extrinsic CH Gerö band photon flux is a factor 2.4 smaller for ethane than for methane. This is close to 2.6 observed in experiments without surface [11] and attributed to different CH radical production rates for methane and ethene. The $CIII$ photon flux is comparable for all cases which reflects the similar carbon balance for both injected species.
- The penetration depths for different break-up products are recorded. The CH penetration depth of $0.44mm$ is comparable for all 4 cases. The C_2 penetration depth varies due to the different origin of the carbon dimer - dissociation during the break-up into C_2 or release as C_2Hy from the surface. The penetration depth profile of CII is shifted and broadened with respect to neutral species. The CII penetration depth for tungsten is longer than for graphite indicating the additional contribution of reflecting carbon ions in the case of tungsten.
- Two types of carbon layers have been identified: build-up prior to and during the injection. A transient carbon coverage (thin layer) of the tungsten limiter surface has been observed in the reference plasma phase though the limiter was positioned in the erosion zone. Secondly, a transient carbon layer was build up by local deposition during the injection. Both layers are eroded by plasma impact and lead e.g. in the case of ethene to substantial C_2Hy release and emission of C_2 Swan band. In contrast to experiments with negligible surfaces - here, transient layers play a significant role and can affect the spectroscopic interpretation.
- Local injection of hydrocarbon species increases the sputtering of W at the surface due to break-up products.

Main results from post mortem analysis can be summarised as follows:

- A factor two difference in the deposition efficiency of ^{13}C for both injected species is found which confirms the substrate dependence of the deposition efficiency observed for methane [20]. The key factors of the substrate effect, under comparable surface roughness, are higher kinetic reflection coefficients of carbon on tungsten than on graphite, and enhanced physical sputtering of carbon deposited on tungsten limiter.
- Carbon layers induced by $^{13}CH_4$ and $^{13}C_2H_4$ injection differ in the layer thickness and the area of the deposit, though a comparable amount of ^{13}C was introduced. The ^{13}C deposition efficiency for ethene is increased up to a factor 1.5 despite the smaller deposit area. The deposit which results from $^{13}C_2H_4$ is more oriented in direction of the $E \times B$ drift indicating a smaller impact of the SOL flows on the transport of corresponding ionic break-up products. Higher sticking of the break-products can also contribute to the larger ^{13}C deposition efficiency in the case of the $^{13}C_2H_4$ injection.

The experiments presented here provide a set of data which will be applied to model both the molecular break-up of hydrocarbon species (methane and ethane) in the plasma as well as erosion and deposition behaviour on the limiter surface (tungsten and graphite).

Acknowledgments

This work was done in the frame of the European Task Force on Plasma-Wall Interaction and the IEA TEXTOR-Japan agreement.

6 References

[1] G. Federici et al., Nucl. Fusion 41 (2001) 1967

[2] A. Kirschner et al., Nucl. Fusion 40 (2000) 989

[3] W. Bohmeyer et al., J. of Nucl. Mater. 337-339 (2005) 89

[4] A. Kreter et al., Plasma Phys. Control. Fus. 50 (2008) 095008

[5] S. Brezinsek et al., J. of Nucl. Mater. 337-339 (2005) 1058

[6] G. Counsel et al., Plasma Phys. Control. Fus. 48 (2006) B198

[7] K. Krieger et al., this conference

[8] M. Mayer et al. J. of Nucl. Mater. 390-391 (2009) 538

[9] Y. Ueda et al., J. of Nucl. Mater. 390-391 (2009) 44

[10] S. Droste et al., Plasma Phys. Control. Fus. 50 (2008) 015006

[11] S. Brezinsek et al., J. of Nucl. Mater. 363-365 (2007) 1119

[12] R. Ding et al., Plasma Phys. Control. Fus. 51 (2009) 055019

[13] B. Schweer et al., Fusion, Science and Tech. 47 (2005) 138

[14] S. Brezinsek et al., Plasma Phys. Control. Fus. 47 (2005) 615

[15] O. Schmitz et al., Plasma Phys. Control. Fus. 50 (2008) 6115004

[16] S. Brezinsek et al., Plasma Fusion Research 3 (2008) 1041

[17] A. Pospieszczyk et al., J. of Nucl. Mater. 241-243 (1997) 883

[18] R. Janev and D. Reiter, Juel-Report 3966 and 4005, www.eirne.de

[19] A. McLean et al., J. of Nucl. Mater. 390-391 (2009) 160

[20] A. Kreter et al., Plasma Phys. Control. Fus. 48 (2006) 1401

Figure captions:

Fig. 1: Photographs of the four spherical limiter installed in the PWI facility in TEXTOR: two graphite (left side) and two tungsten limiters (right side) were subsequentially exposed to deuterium plasma. The ^{13}C deposition pattern around the injection aperture is caused by local injection of $^{13}C_2H_4$ (upper two limiters) and $^{13}CH_4$ (lower two limiters).

Fig. 2: Edge plasma parameters deduced from the He beam diagnostic located at the outer midplane for a discharge with graphite limiter and $^{13}C_2H_4$ injection and with $^{13}CH_4$, respectively. The edge electron temperature and density within each discharge series as well as between different series are well reproducible.

Fig. 3: a) CD/CH A-X band photon flux density in front of the graphite (upper images) and tungsten limiter (lower images) in discharges with $^{13}C_2H_4$ injection. The first image in each row represents the intrinsic CD emission at the strike-zone prior to injection. The second shows the sum of intrinsic CD and extrinsic CH emission resulting from the break-up of the injected species. The third image shows the difference image and reflects the extrinsic CH emission due to injection. b) Toroidal integration of the CD/CH A-X band photon flux density in a narrow stripe around the injection aperture gives the corresponding penetration depth profiles. c) Time evolution of the spatially integrated CD/CH A-X band in discharges with $^{13}C_2H_4$ injection through graphite and tungsten limiter, respectively. CII, $CIII$ and C_2 d-a band photon fluxes are shown for reference.

Fig. 4: 2D distribution of extrinsic hydrocarbon break-up products (CH, C_2, C^+ and C^{2+}) during the catabolism of injected $^{13}C_2H_4$ (upper images) and $^{13}CH_4$ (lower images) in deuterium plasma. The photon flux densities in front of the graphite limiter were recorded with an intensified CCD camera equipped with narrowband interference filters for CD/CH,

C_2, CII, and $CIII$ as specified in section 3.2.

Fig. 5: a) Radially resolved spectra recorded during the extrinsic phase with $^{13}CH_4$ and $^{13}C_2H_4$ injection, respectively, in front of the graphite and tungsten limiter, respectively. The CH Gerö band head at $431.4nm$ and the CII doublet at $426.7nm$, observed in spectral region (i), and the C_2 Swan band head at $516.5nm$ as well as the CII mulitplet at $515.0nm$, observed in spectral region (ii), are indicated. For tungsten also WI lines are marked. The dashed lines indicate the position of the aperture embedded in the limiters. b) Normalised penetration depth profiles of the CH Gerö band, the C_2 Swan band, and two CII lines observed at the toroidal position of the aperture and integrated over $1mm$.

Fig. 6: a) The ^{13}C deposition pattern on the limiter surfaces with comparable roughness for the four cases obtained by NRA. b) The ^{13}C and D areal density along the line of maximum emission, which is indicating in a).

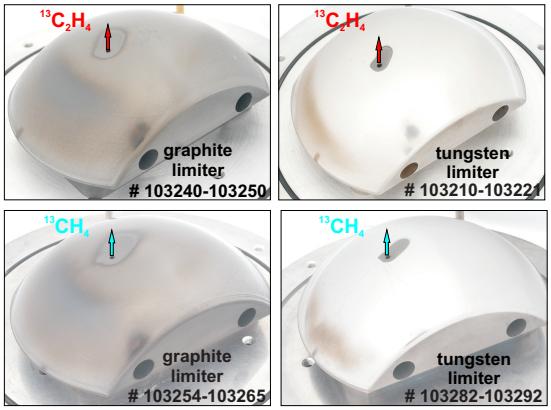

Figure 1:

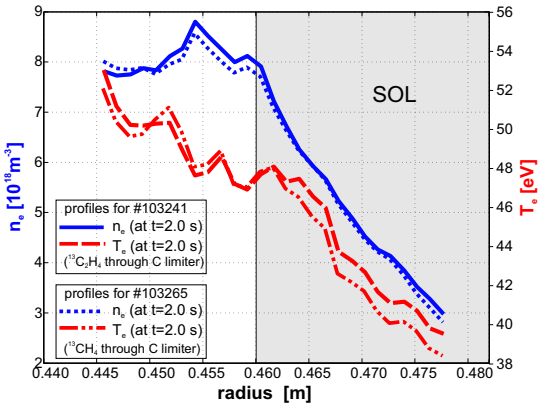

Figure 2:

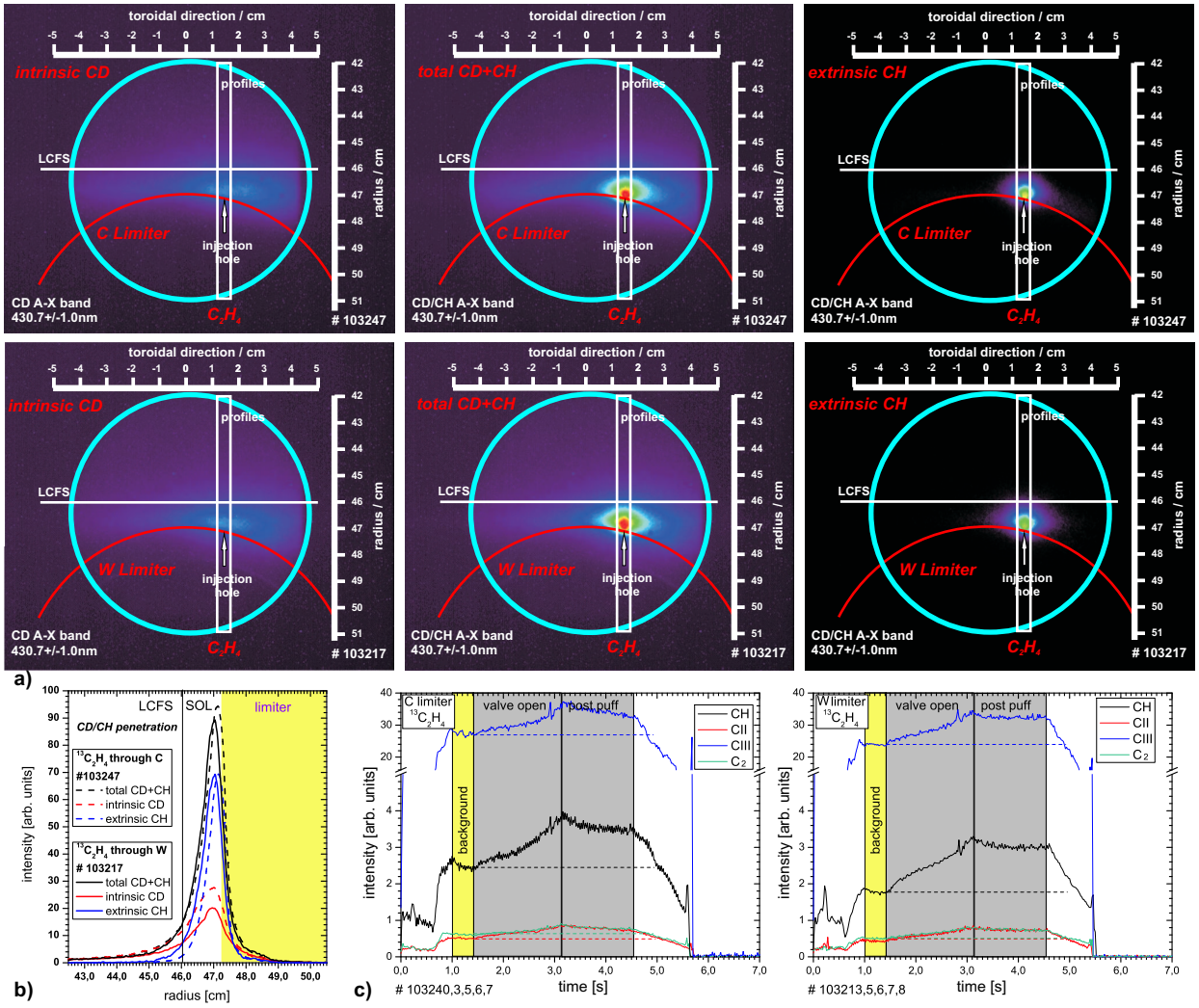

Figure 3:

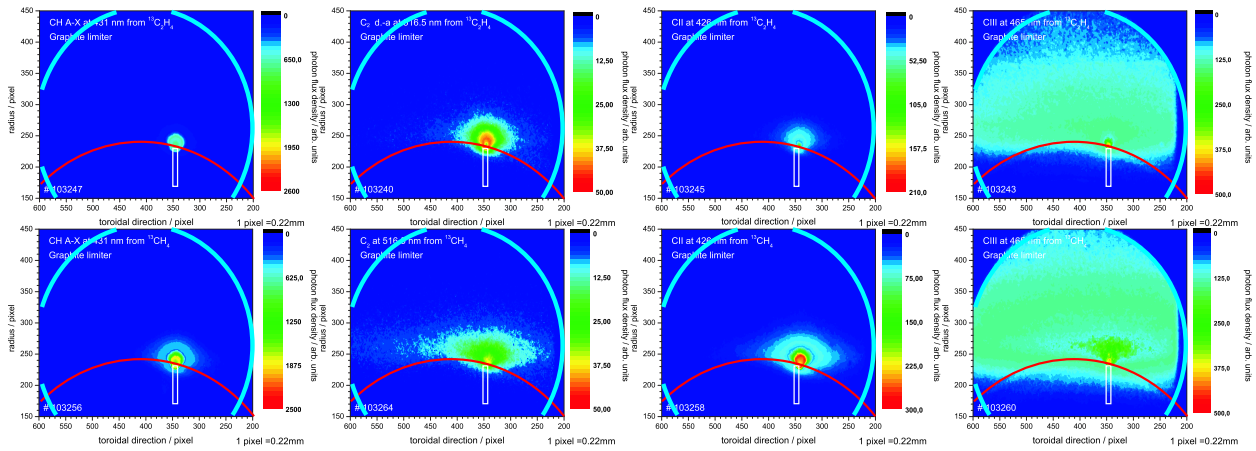

Figure 4:

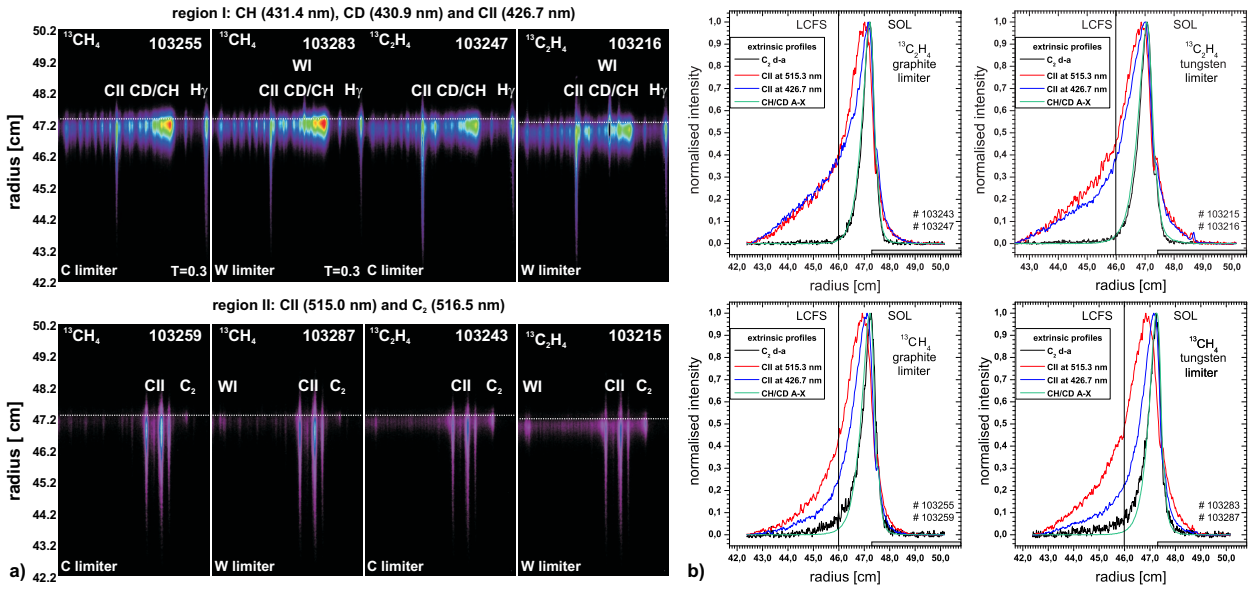

Figure 5:

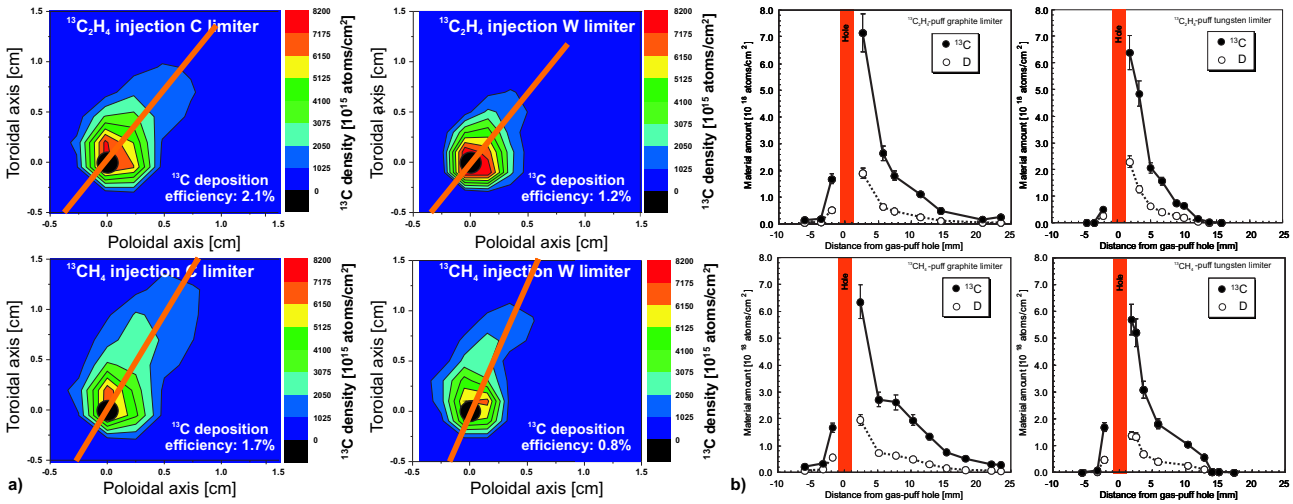

Figure 6: